Evaluating the Impacts of Microgrids & Automation on Distribution System Reliability and Resiliency

M Al Mamun[1], Monish Mukherjee[1], Priya T Mana[1], Frank Tuffner[1], Kenneth Wilhelm[2], Zoe Oens[2], Derek Hansen[2], and Michael Diedesch[2]
[1]Pacific Northwest National Laboratory, Richland, WA, USA
[2]Avista Corporation, Spokane, WA, USA

***Abstract*—The evolving demands for improved reliability and resilience in power systems have driven the integration of advanced technologies such as microgrids and distribution automation into distribution networks. Microgrids (MGs) offer a practical solution, integrating distributed generation and energy storage to autonomously supply localized power when the broader grid is compromised. Coupled with advanced automation technologies MGs enable utilities to perform rapid fault isolation, resilient load restoration, and coordinated recovery. Despite demonstrated improvements, assessing the true impacts of MGs and automation on reliability and resilience remains complex due to stochastic outputs of distributed local resources, dynamic outage scenarios, and the limitations of existing metrics. To address these challenges, this paper presents an mixed-integer linear programming (MILP) based Distribution Service Restoration (DSR) approach that incorporates temporal variation of demand, generation, storage availability to optimize switching operations, DER dispatch, load prioritization, and MG island formation during outages and thereby reflect the true performance of MGs and automation. The proposed approach is in integrated with standardized reliability metrics and resilience measures to present an assessment framework to evaluate the impacts of MG integration and automation in distribution networks, facilitating utility investment decisions and enabling efficient system-level planning for enhanced reliability and resilience.**

***Index Terms*—Microgrids, reliability, resilience, restoration, distributed generators, mixed integer linear programming**

I. INTRODUCTION

Distribution grids are facing challenges from infrastructure aging and extreme weather events. In such situations, microgrids (MGs) provide utilities with practical solutions for improving distribution reliability and resilience [1]. A microgrid is a localized electrical system, integrating distributed resources, energy storage, and controllable loads, capable of operating in either grid-connected or islanded mode. By autonomously managing voltage, frequency, and power flow, MGs enable utilities to maintain service to critical loads during emergency conditions [2], [3]. When coupled with advanced distribution automation, such as intelligent electronic devices (IEDs), automated switches, real-time sensing, and ADMS, MGs function as strategic operational assets [4], [5]. This transforms MGs into utility-operated resilience cells when the broader grid is compromised.

Distribution service restoration (DSR) leveraging MGs combined with advanced automation has been extensively studied [6]–[10]. These studies on DSR have focused on determining the sequence of control actions (e.g. switching, MG formation and asset dispatch) that can restore customers after a fault and presented approaches span from heuristic rule-based strategy [6], cluster-based models [8], to mixed integer linear programming (MILP) [9], [10]. Most commonly adopted DSR approaches involve MILP to jointly optimize switching operations, DER dispatch, load pickup, and MG-island formation, while enforcing radiality, voltage, and thermal constraints [7], [11]. However, effective DSR requires coordinating the operation of MGs and switching actions over the expected outage horizon and existing approaches have limitations in incorporating some variables that are changing over time including demand, generation & storage availability [12].

Furthermore, assessing the true impact of MG and automation on system reliability and resilience presents significant challenges for utilities towards justifying investment costs. Quantifying such impact is inherently complex because of stochastic DER outputs, variable load profiles, and complex outage scenarios [13], [14]. While some efforts have presented reliability assessment approaches [15], reliability metrics such as SAIDI & SAIFI fail to capture the full spectrum of resilience benefits. Towards quantifying resilience, some existing studies have presented probabilistic and scenario-based approaches [16]. However, the lack of standardized resilience metrics and computational complexities of the analyses limits their practical implementation for utility decision-making [13]. Even if MG and automation can enhance reliability & resilience, quantifying their impact remains a complex task.

To overcome this challenge, this paper presents an assessment framework for evaluating the impacts of microgrids and automation in enhancing the reliability & resilience of distribution systems. It develops an enhanced MILP-based DSR approach that incorporates temporal variation in estimated demand, generation, and storage availability to determine the sequence of DSR control actions restoring maximum possible customers throughout the predicted outage duration. The study integrates the DSR approach with outage scenarios and standardized metrics to evaluate the impacts in improving reliability and resilience. The key contributions are: (1) an enhanced DSR approach that captures the true restoration performance of microgrids and (2) an assessment approach to separately quantify the improvements in resiliency and reliability and, thereby, facilitate utilities with investment decision-making.

II. QUANTIFYING RELIABILITY AND RESILIENCE

Reliability in electric power systems is the ability of the grid to deliver electricity continuously with minimal interruptions, reflecting both resource adequacy and system security. Quantification of reliability has been standardized through IEEE

This material is based on work supported by the U.S. Department of Energy (DOE), Microgrids R&D Program. Pacific Northwest National Laboratory is operated for DOE by the Battelle under Contract DE-AC05-76RL01830.

979-8-3315-8138-1

1366 reliability indices: SAIFI (average number of sustained outages per customer), SAIDI (total outage duration per customer), CAIDI (restoration time per interruption) [17]. These indices have become the industry standard, widely adopted by utilities and regulators for benchmarking, performance reporting, and reliability-focused investment planning. IEEE 1366 also defines Major Event Days (MEDs) using the Beta method to exclude statistically abnormal outage days from routine metrics, ensuring fair performance assessment.

$$\text{SAIDI} = \frac{\text{Total Customer Minutes of Interruption}}{\text{Total Number of Customers Served}} \tag{1}$$

$$\text{SAIFI} = \frac{\text{Total Number of Customers Interrupted}}{\text{Total Number of Customers Served}} \tag{2}$$

$$\text{CAIDI} = \frac{\text{Total Customer Minutes of Interruption}}{\text{Total Number of Customers Interrupted}} = \frac{\text{SAIDI}}{\text{SAIFI}} \tag{3}$$

Using reliability metrics presents several challenges in the assessment of resilience as they were designed to measure performance under routine operating conditions, not the system's ability to withstand, adapt, and rapidly recover from high-impact, low frequency (HILF) events i.e. Resilience. IEEE 1366's treatment of MEDs intentionally excludes extreme events from standard reliability calculations, making these metrics insufficient for evaluating resilience improvements from upgrades like microgrids and automation. Resilience also involves dynamic system behaviors like islanding, recovery, and the temporal evolution of outages that are not captured by existing indices. As a result, utilities and regulators face a gap between measurable reliability and resilience performance, complicating cost justification and investment prioritization.

Towards addressing that gap, the IEEE Distribution resilience Working Group (WG) has defined resilience as "*the capability of electric power distribution systems to deliver electric energy to end-use customers by avoiding interruptions and/or recovering this capability following exposure to naturally occurring HILF events*". The WG has also proposed a set of resilience metrics to capture operational performance of a system during HILF events: Sustained Interruption Reduction Index (SIRI) - evaluate the effectiveness of automation in preventing customer interruption (CI), Restoration Effectiveness (RE) - focuses on reductions in the number of customers without power for more than a threshold "H" hours and REPAIR - evaluates the effectiveness of event response team organization and scheduling, as given by (4).

$$\text{SIRI} = \frac{\text{Avoided Sustained CI by Automation/Hardening}}{\text{Avoided Sustained CI by Automation/Hardening + Sustained CI}} \tag{4}$$

$$\text{RE-H} = \frac{\text{Customer without power for more than H hours}}{\text{Avoided Sustained CI by Automation/Hardening + Sustained CI}} \tag{5}$$

$$\text{REPAIR} = \log\left(\frac{\text{CrewHours}}{\text{Outages}} \cdot \frac{\text{AUPC}}{\text{CI}}\right) \tag{6}$$

Where *CrewHours* denotes the total hours spent on the field by crew and *AUPC* is the area under the restoration curve which reflects the tracked restoration efforts vs emerging outages.

III. Service Restoration with Microgrids

This section illustrates the adopted method for resilient restoration of distribution systems using microgrids as follows.

A. Restoration Problem Definition

A radial distribution system with n number of three-phase nodes is represented using a directed graph $\mathcal{G} = (\mathcal{V}, \mathcal{E})$,

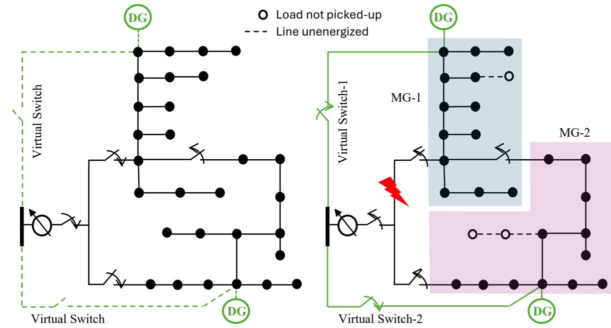

(a) Normal operational system (b) Reconfigured system after an extreme event

Fig. 1. Restoration process with an example feeder.

where $\mathcal{V} = \{1, 2, \ldots, n\}$ is the set of available nodes and $\mathcal{E} = \{(i,j)|i,j \in \mathcal{V}\}$ is the set of connected branches. To restore loads after an extreme event, the original system graph can be divided into m number of radial sub-graphs with m being the number of distributed generators (DGs), for example, battery energy storage systems (BESSs), as shown in Fig. 1.

In the restoration method, a DG is considered to be connected to the substation through a virtual switch (vsw). During the normal operation as shown in Fig. 1 (a), DGs remain inactive and the loads are supplied by the substation. After an event, the proposed DSR approach first isolates the fault location so that the fault is not fed from any direction. If the fault isolation process disconnects the substation from the feeder, the optimization method may close the virtual switches and the DGs come into action to restore loads, creating self-sustained microgrids (MGs). The formulation ensures that reconfigured topology for each MG, including DGs and loads, is radially connected, as illustrated in Fig. 1 (b). Note that vsw is introduced only for developing the optimization model for the DSR problem and doesn't exists in real system.

The restoration problem is formulated as a multi-period mixed-integer linear program (MILP) by linearizing the system nonlinear constraints to obtain the global optimal solution and speed-up the computation, with a multi-objective of maximizing the amount of load served and minimizing the switching operation of the smart switches in the system as given in (7). Here, $P^{\tau}_{L,i}$ is the active load at node i at time τ, $\mathcal{C}_{L,i} \in 0,1$ is the load-criticality, γ_i and δ_{ij} refer to the binary decision variables for γ_i and the branch $i \rightarrow j$. w_1 and w_2 represent weight factors of the two objective functions which enables a configurable prioritization between maximizing load pickup and minimizing the number of switching actions.

$$\textbf{Max}\text{:}\; w_1 \sum_{\tau \in \mathcal{T}} \sum_{i \in \mathcal{N}} \gamma_i\, \mathcal{C}_{L,i} P^{\tau}_{L,i} - w_2 \sum_{ij \in \mathcal{E}} \delta_{ij} \tag{7}$$

B. Restoration Problem Constraints

After the fault is isolated, all possible radial feeders (with respect to the substation) are generated by performing combinations of tie switches, sectionalizing switches and virtual switches as described in [10]. The restoration method would select one of these radial feeders. For a particular feeder, the restoration method considers nodes, branches and loads with binary status (connected or disconnected), which are represented by v, s and δ respectively. In addition, these are

979-8-3315-8138-1

the fixed variables irrespective of the number of simulation intervals. Now, to form a microgrid, the DG connected node must be energized. In addition, to make sure a radial power flow from parent to child nodes, maximum one DG needs to be enabled. These are given by the constraint in (8), where $\mathcal{M}$ is the set of available DGs in the system.

$$v_i^k = 1, \sum_{\forall k \in \mathcal{M}} v_i^k \leq 1 \qquad \forall k \in \mathcal{M}, \forall i \in \mathcal{V} \tag{8}$$

If a load is to be served or not, the load node must be energized, which is enforced by $\gamma_i = v_i \ s_i$. However, this is a multiplication of two binary variables and, hence, nonlinear term, which is linearized in (9), $\forall i \in \mathcal{V}, \forall k \in \mathcal{M}$.

$$\gamma_i^k \leq v_i^k, \ \gamma_i^k \leq s_i^k, \ \gamma_i^k \geq v_i^k + s_i^k - 1 \tag{9}$$

Radial topology is ensured in (10) where ψ is the set of child nodes, whereas (11) ensures uncontrolled switches are always energized and unavailable branches are not energized.

$$v_j^k - v_i^k \leq 0, \ \forall j \in \psi, \forall i \in \mathcal{V}, \forall k \in \mathcal{M} \tag{10}$$

$$v_i^k - v_j^k = 0, v_i^k + v_j^k \leq 1, \forall j \in \psi, \forall i \in \mathcal{V}, \forall k \in \mathcal{M} \tag{11}$$

The energy capacity of a DG is denoted as the state of charge (SOC) being defined in (12), where $\tau \in \mathcal{T}$ (set of simulation time intervals in hours), P_c and P_d are charging and discharging power of DG, Δt indicates interval duration, η_c and η_d denote the charging and discharging efficiencies, respectively and E_{dg} is the rated capacity of a DG.

$$SOC^{k,\tau} = SOC^{k,\tau-1} + \left(\eta_c P_c^{k,\tau} - \eta_d P_d^{k,\tau}\right) \Delta t / E_{dg}^k \tag{12}$$

Charging and discharging power, P_c and P_d, are bounded as given in (13), where P_c^{max}, P_d^{max} are maximum charging and discharging power with u_c and u_d being the corresponding associated binary decision variables respectively.

$$\begin{aligned} &P_c^{k,\tau} \leq P_c^{max} \, u_c^{k,\tau}, \ P_c^{k,\tau} \geq 0, \forall k \in \mathcal{M}, \forall \tau \in \mathcal{T} \\ &P_d^{k,\tau} \leq P_d^{max} \, u_d^{k,\tau}, \ P_d^{k,\tau} \geq 0, \forall k \in \mathcal{M}, \forall \tau \in \mathcal{T} \end{aligned} \tag{13}$$

DG active output power P_{dg} is defined in (14).

$$P_{dg}^{k,\tau} = P_d^{k,\tau} - P_c^{k,\tau}, \forall k \in \mathcal{M}, \forall \tau \in \mathcal{T} \tag{14}$$

The reactive power of DG, $Q_{dg} = \sqrt{S_{dg}^2 - P_{dg}^2}$ with S_{dg} being the rated power. However, this is a nonlinear equation and, hence, it is linearized by the set of Octagon constraints in (15), where $c_f = \sqrt{2} - 1$ is the coefficient of the Octagon constraints and $\mathcal{S}_{dg}$ is the rated active power of DG.

$$\begin{aligned} &Q_{dg}^{k,\tau} \leq \mathcal{S}_{dg}^k, \ Q_{dg}^{k,\tau} \geq -\mathcal{S}_{dg}^k \\ &c_f \, P_{dg}^{k,\tau} + Q_{dg}^{k,\tau} \leq \mathcal{S}_{dg}^k, \ c_f \, P_{dg}^{k,\tau} - Q_{dg}^{k,\tau} \leq \mathcal{S}_{dg}^k \\ &P_{dg}^{k,\tau} + c_f \, Q_{dg}^{k,\tau} \leq \mathcal{S}_{dg}^k, \ P_{dg}^{k,\tau} - c_f \, Q_{dg}^{k,\tau} \leq \mathcal{S}_{dg}^k \end{aligned} \tag{15}$$

The distribution of P_{dg} and Q_{dg} over three phases is defined in (16), making the DG provide unbalanced power. Here, a, b and c are the three phases of a node.

$$P_{dg,a}^{k,\tau} + P_{dg,b}^{k,\tau} + P_{dg,c}^{k,\tau} = P_{dg}^{k,\tau}, Q_{dg,a}^{k,\tau} + Q_{dg,b}^{k,\tau} + Q_{dg,c}^{k,\tau} = Q_{dg}^{k,\tau} \tag{16}$$

The per-phase active power of a DG is tightened in (17).

$$\begin{aligned} &P_{dg,a}^{k,\tau} \leq \mathcal{P}_{dg}^k \, u_d^{k,\tau}, \ P_{dg,b}^{k,\tau} \leq \mathcal{P}_{dg}^k \, u_d^{k,\tau}, \ P_{dg,c}^{k,\tau} \leq \mathcal{P}_{dg}^k \, u_d^{k,\tau} \\ &P_{dg,a}^{k,\tau} \geq -\mathcal{P}_{dg}^k \, u_c^{k,\tau}, \ P_{dg,b}^{k,\tau} \geq -\mathcal{P}_{dg}^k \, u_c^{k,\tau}, \ P_{dg,c}^{k,\tau} \geq -\mathcal{P}_{dg}^k \, u_c^{k,\tau} \end{aligned} \tag{17}$$

The per-phase reactive DG power is also constricted as in (18).

$$Q_{dg,a}^{k,\tau} \leq \mathcal{P}_{dg}^k, \ Q_{dg,b}^{k,\tau} \leq \mathcal{P}_{dg}^k, \ Q_{dg,c}^{k,\tau} \leq \mathcal{P}_{dg}^k \tag{18}$$

Solar PV inverters inject active power according to dynamic solar irradiance, where $\mathcal{Z}$ is the set of available PV inverters and $\mathcal{P}_{pv}$ is the available active PV power.

$$P_{pv}^{l,\tau} \leq \mathcal{P}_{pv}^l, \ \ Q_{pv}^{l,\tau} \leq \mathcal{P}_{pv}^l, \ \forall l \in \mathcal{Z} \tag{19}$$

Reactive power of PVs is calculated as $Q_{pv} = \sqrt{\mathcal{S}_{pv}{}^2 - P_{pv}^2}$ with S_{pv} being the PV inverter rating which is limited by $\mathcal{P}_{pv}^l$. This is linearized using the Octagon constraints given by (20).

$$\begin{aligned} &c_f \, P_{pv}^{l,\tau} + Q_{pv}^{l,\tau} \leq \mathcal{P}_{pv}^l, \ c_f \, P_{pv}^{l,\tau} - Q_{pv}^{l,\tau} \leq \mathcal{P}_{pv}^l \\ &P_{pv}^{l,\tau} + c_f \, Q_{pv}^{l,\tau} \leq \mathcal{P}_{pv}^l, \ P_{pv}^{l,\tau} - c_f \, Q_{pv}^{l,\tau} \leq \mathcal{P}_{pv}^l \end{aligned} \tag{20}$$

Network power flows are time coupled and get updated each time instant or interval as the simulation continues. Network power flow is solved by using the Simplified DistFlow method [18], a linear power flow solver, as given in (21)-(23), where p and q denote active and reactive branch flows, P_L and Q_L are active and reactive loads, V represents node voltage magnitude, r and x are resistance and reactance of a branch, and V_o is the nominal voltage magnitude of the DG connected node. The set of following power flow equations are valid $\forall (i, j, \alpha) \in \mathcal{V}$, $\forall \tau \in \mathcal{T}$, and $\forall l \in \mathcal{Z}$. Also, $\zeta_j^l = 1$ if $j \in z$, and 0 otherwise, where z is the set of PV nodes.

$$p_{i \to j}^{k,\tau} = \gamma_j^k \ P_{L,j} + \sum_{j \to \alpha \in \mathcal{E}, i \neq \alpha} p_{j \to \alpha}^{k,\tau} - \zeta_j^l \, P_{pv}^{l,\tau} \tag{21}$$

$$q_{i \to j}^{k,\tau} = \gamma_j^k \ Q_{L,j} + \sum_{j \to \alpha \in \mathcal{E}, i \neq \alpha} q_{j \to \alpha}^{k,\tau} - \zeta_j^l \, Q_{pv}^{l,\tau} \tag{22}$$

$$V_j^{k,\tau} = V_i^{k,\tau} - (r_{ij} \ p_{i \to j}^{k,\tau} + x_{ij} \ q_{i \to j}^{k,\tau}) / V_o^k \tag{23}$$

When a microgrid is formed, the restoration method enables the corresponding MG (see Fig. 1) and the power flow through this switch should be equal to the DG power, as defined in (24) with V_{sub} being the substation bus voltage, assuming that $i \to j = 1 \to 2$ is the parent branch in the radial microgrid.

$$V_1 = V_{sub}, \, p_{1 \to 2}^{k,\tau} = P_{dg}^{k,\tau}, \, q_{1 \to 2}^{k,\tau} = Q_{dg}^{k,\tau} \ \forall k \in \mathcal{M}, \forall \tau \in \mathcal{T} \tag{24}$$

Node voltage magnitudes should be within the minimum (V_{min}) and maximum (V_{max}) bounds as shown in (25).

$$v_i^k \ V_{min} \leq V_i^{k,\tau} \leq v_i^k \ V_{max}, \forall i \in \mathcal{V}, \forall k \in \mathcal{M}, \forall \tau \in \mathcal{T} \tag{25}$$

IV. Numerical Results

The restoration approach is implemented on the modified IEEE 123-Node Test Feeder in Fig. 2. The system has normally closed (NC) switches between buses 150-149, 13-152, 18-135 and 97-197, and normally open (NO) tie-switches between 47-250 and 35-66. The test case involves two DGs, DG-1 at node 40 and DG-2 at node 67. DG-1 and DG-2 are rated 450 kW and 400 kW respectively. Both DGs have capacity of 2.25 MWh. The test case also includes two PV systems, PV-1 at node 41 and PV-2 at node 68, each rated 200 kW. System dynamic load multipliers and solar irradiance for a typical summer day are shown in Fig. 3. Since criticality of the loads were not known, the DGs were assumed to be placed near the

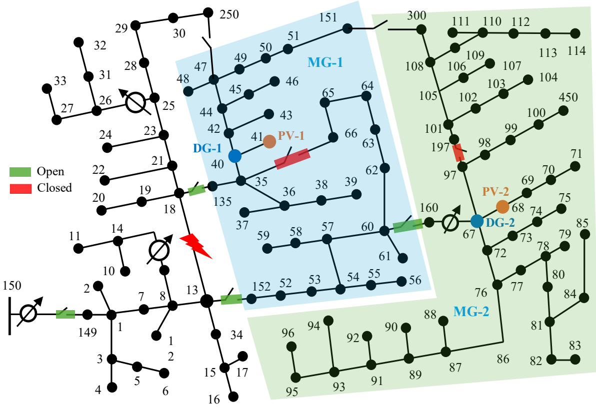

Fig. 2. Modified IEEE 123 Node system along with a reconfigured topology

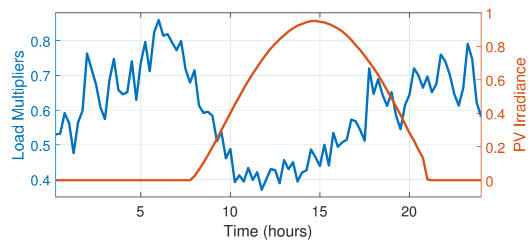

Fig. 3. Load and PV profiles

critical loads and $\mathcal{C}_{L,i}$ in (7) was considered to be uniform for all the loads. Considered weights in (7) are $w_1 = 100$ and $w_2 = 1e^{-6}$, giving more priority to maximize the load served. The proposed DSR model is developed on Python 3.12 and solved by Gurobi solver [19] with the MIPGap of 0.75%.

A. Performance of Proposed Restoration Method

To demonstrate the performance of the proposed DSR model, an extreme weather event is assumed to happen on line 13-18 at 9 AM for 8 hours. At the very first step, the restoration method isolates the fault by opening the NC switches 150-149, 13-152 and 18-135, disconnecting the substation from the rest of the grid. Once the fault is isolated, the algorithm generates all possible combinations of radial feeders with respect to the substation, while considering the virtual switches between DG nodes and the substation. Then, the DSR model is solved to determine the optimal reconfiguration. The topological solutions (whether connected or disconnected) regarding nodes, branches and loads remain unchanged throughout the simulation intervals, which is shown in Fig. 2. However, the dispatches from DGs, PVs and the substation changes over each time interval the restoration model is solved.

From the optimal reconfiguration solution (see Fig. 2), it is seen that the NC switches 60-160 and 61-610 are open, while closing the NO tie-switch 35-66. Thus, both DGs are enabled to make self-sustained microgrids, MG1 (shaded blue) and MG2 (shaded green) led by DG-1 and DG-2 respectively. Dispatches from DGs and PVs are shown in Fig. 4. As the restoration model prioritizes full utilization solar energy, active power injections from PV exactly follow the solar irradiance as given in Fig. 3. Consequently, active power from DGs keeps decreasing as PV rises. It is noticed that dispatches from PVs are identical, whereas DG dispatches vary. This is because both PVs follow the same solar irradiance profile, whereas

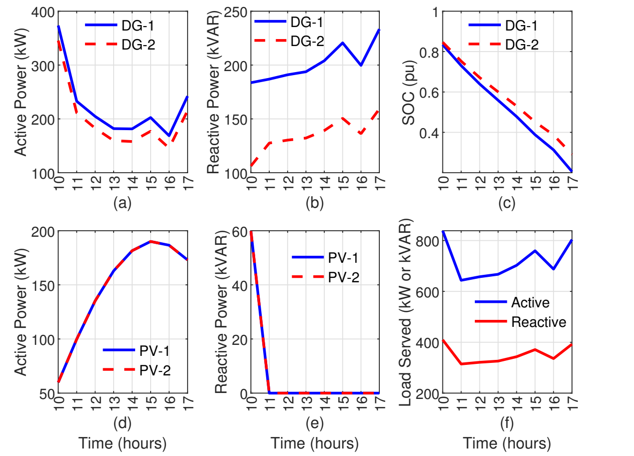

Fig. 4. MG dispatches: (a)-(c) dispatch from DGs, (d)-(e) dispatch from PVs, and (f) load served by the MGs.

TABLE I
FAULT AND RECONFIGURATION (MG: MICROGRID)

Fault Info		Reconfiguration Solution		
Line	Hours	Switch to Open	Switch to Close	MWh
13-18	1	150-149,13-152,18-135,60-160,97-197	MG1, MG2,151-300,35-66	0.85
	3	150-149,13-152,18-135,60-160,97-197	MG1, MG2,151-300,35-66	2.16
	5	150-149,13-152,18-135,60-160,97-197	MG1, MG2,151-300,35-66	3.54
	7	150-149,13-152,18-135,60-160,97-197	MG1, MG2,151-300,35-66	5.00
	9	150-149,13-152,18-135,97-197	MG1, MG2,151-300	6.57
	15	150-149,13-152,18-135,60-160	MG1, MG2,35-66	7.14
	21	150-149,13-152,18-135,97-197	MG1, MG2,151-300	6.81
74-75	1	13-152,60-160,97-197	151-300, 35-66	0.09
	2	18-135,60-160,97-197	151-300, 47-250	0.22
	4	60-160,97-197	151-300	0.57
	6	18-135,60-160,97-197	151-300, 47-250	0.99
	8	13-152,18-135,60-160,97-197	151-300, 47-250,35-66	1.41
	14	18-135,60-160,97-197	151-300, 47-250	1.57
	22	18-135,60-160,97-197	151-300, 47-250	1.57
30-250	1	150-149,13-152,18-135,60-160,97-197	MG1, MG2,151-300,35-66	0.85
	2	150-149,13-152,18-135,60-160,97-197	MG1,MG2, 151-300,35-66	1.50
	4	150-149,13-152,18-135,60-160,97-197	MG1,MG2, 151-300,35-66	2.83
	6	150-149,13-152,18-135,60-160,97-197	MG1,MG2,151-300,35-66	4.31
	8	150-149,13-152,18-135,60-160,97-197	MG1,MG2, 151-300,35-66	5.82
	14	150-149,13-152,18-135,60-160,97-197	MG1,MG2, 151-300,35-66	7.13
	22	150-149,13-152,18-135,60-160,97-197	MG1,MG2, 35-66	6.62
108-300	1	18-135,97-197	47-250	0.12
	2	18-135,97-197	47-250	0.32
	4	13-152,97-197	35-66	0.92
	6	18-135,97-197	47-250	1.66
	8	13-152,18-135,97-197	47-250, 35-66	2.38
	14	18-135,97-197	47-250	3.14
	22	18-135,97-197	47-250	3.14
64-65	1	13-152,60-160	151-300	0.12
	3	13-152,18-135,60-160	151-300, 47-250	0.59
	5	13-152,60-160	151-300	1.28
	7	13-152,18-135,60-160	151-300, 47-250	2.03
	9	13-152,18-135,60-160	151-300, 47-250	2.68
	15	13-152,18-135,60-160	151-300, 47-250	3.14
	21	13-152,18-135,60-160	151-300, 47-250	3.14

DG dispatch depends on the amount of load being restored, which may differ. Reactive dispatches from DGs and PVs are optimally determined to maintain system voltage constraints. DG SOCs are in Fig. 4 (c) keeps declining as they continue serving loads. The total load served, as shown in Fig. 4 (f), follows the similar trend of DG dispatch. The reason behind this is DG dispatches vary as per the load profile, which is the lowest during this fault duration, completely utilizing PVs.

B. Improvements on Reliability and resilience metrics

Thirty events are created to occur on lines 13-18, 152-52, 30-250, 108-300 and 64-65 at 9 AM on thirty different days.

979-8-3315-8138-1

TABLE II
RELIABILITY AND RESILIENCE METRICS

Metrics	Base Case	DA	MG & DA
Reliability Metrics			
SAIDI (All Event Days)	10804.91	8747.59	6570.56
SAIFI (All Event Days)	21.36	16.96	11.59
CAIDI (All Event Days)	505.85	515.78	566.92
SAIDI (Non Major Event Days)	1365.65	1010.65	826.57
SAIFI (Non Major Event Days)	7.95	5.91	4.12
CAIDI (Non Major Event Days)	171.78	171.01	200.62
resilience Metrics			
SIRI (Major Event Days)	N/A	0.175	0.44
RE-12 (Major Event Days)	0.44	0.37	0.29

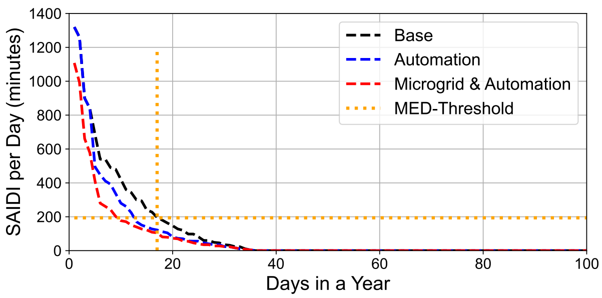

Fig. 5. SAIDI with the base case and microgrids.

The fault information and the optimal reconfiguration solution with MWh served are shown in Table. I. It is observed that MGs are formed for the faults on lines 13-18 and 30-250 as the fault isolation process fully disconnects the substation. Whereas, substation remains connected for the other cases to supply loads and, hence, MGs are not formed. Also, it is seen that MGs help serve more MWh for longer fault durations.

Improvement on reliability and resilience metrics is demonstrated with a list of faults given in Table I for three scenarios: base case, automation with smart switches, and automation with microgrids. Fig. 5 depicts the SAIDI profiles for these three scenarios. It is observed that the restoration with microgrids and automation brings the most significant improvement on SAIDI, compared to the base case with and without automation. In addition, all reliability and resilience metrics determined are given in Table II. It is observed that the microgrid with automation gives the most improved metrics. Only the CAIDI values are increasing, which is because the declining rate of SAIFI is higher than SAIDI.

From a practical standpoint, the metrics can facilitate decision-making between microgrid & automation projects based on the degree of reliability & resiliency improvements as compared to the cost of deployment (*i.e.* cost-benefit ratio).

V. CONCLUSIONS

This paper present an MILP-based framework for Distribution Service Restoration (DSR) that leverages microgrids and automation to enhance distribution system reliability and resilience. By incorporating dynamic system parameters such as demand, DER generation, and storage SOC, the framework optimizes switching operations, DER dispatch, and microgrid island formation during outages. The proposed approach addresses limitations in traditional reliability metrics, introducing probabilistic and scenario-based resilience measures for quantifying impacts. Results demonstrate that microgrids coupled with automation significantly reduce restoration times, prioritize critical loads, and enhance system resilience, providing utilities with actionable insights for investment planning.

Some potential future directions include analyzing the sensitivity of the weight-factors (maximize loads vs minimize switching actions) along with integrating the metrics with interruption costs estimates (ICE- [20]) to evaluate the avoided interruption costs as compared to cost of deployment.

REFERENCES

[1] C. Chen, J. Wang, and D. Ton, "Modernizing distribution system restoration to achieve grid resiliency against extreme weather events: An integrated solution," *Proceedings of the IEEE*, vol. 105, no. 7, 2017.

[2] IEEE, "IEEE standard for the specification of microgrid controllers," 2017.

[3] P. T. Mana, K. P. Schneider, W. Du, M. Mukherjee, T. Hardy, and F. K. Tuffner, "Study of microgrid resilience through co-simulation of power system dynamics and communication systems," *IEEE Transactions on Industrial Informatics*, vol. 17, no. 3, pp. 1905–1915, 2021.

[4] Y. Xu, C.-C. Liu, K. P. Schneider, F. K. Tuffner, and D. T. Ton, "Microgrids for service restoration to critical load in a resilient distribution system," *IEEE Transactions on Smart Grid*, vol. 9, no. 1, pp. 426–437, 2018.

[5] M. A. Igder, X. Liang, and M. Mitolo, "Service restoration through microgrid formation in distribution networks: A review," *IEEE Access*, vol. 10, pp. 46618–46632, 2022.

[6] K. S. A. Sedzro, X. Shi, A. J. Lamadrid, and L. F. Zuluaga, "A heuristic approach to the post-disturbance and stochastic pre-disturbance microgrid formation problem," *IEEE Transactions on Smart Grid*, vol. 10, no. 5, pp. 5574–5586, 2019.

[7] Z. Wang and J. Wang, "Self-healing resilient distribution systems based on sectionalization into microgrids," *IEEE Transactions on Power Systems*, vol. 30, no. 6, pp. 3139–3149, 2015.

[8] J. Li, X.-Y. Ma, C.-C. Liu, and K. P. Schneider, "Distribution system restoration with microgrids using spanning tree search," *IEEE Transactions on Power Systems*, vol. 29, no. 6, pp. 3021–3029, 2014.

[9] C. Chen, J. Wang, F. Qiu, and D. Zhao, "Resilient distribution system by microgrids formation after natural disasters," *IEEE Transactions on Smart Grid*, vol. 7, no. 2, pp. 958–966, 2016.

[10] S. Poudel, A. Dubey, and K. P. Schneider, "A generalized framework for service restoration in a resilient power distribution system," *IEEE Systems Journal*, vol. 16, no. 1, pp. 252–263, 2020.

[11] S. Lei, C. Chen, Y. Song, and Y. Hou, "Radiality constraints for resilient reconfiguration of distribution systems: Formulation and application to microgrid formation," *IEEE Transactions on Smart Grid*, vol. 11, no. 5, pp. 3944–3956, 2020.

[12] B. Chen, C. Chen, J. Wang, and K. L. Butler-Purry, "Multi-time step service restoration for advanced distribution systems and microgrids," *IEEE Transactions on Smart Grid*, vol. 9, no. 6, pp. 6793–6805, 2018.

[13] Y. Yao, R. Jain, and R. Cox, "Quantitative metrics for grid resilience evaluation and optimization," *IEEE Transactions on Sustainable Energy*, 2022.

[14] M. Ibrahim and A. Alkhraibat, "Resiliency assessment of microgrid systems," *Applied Sciences*, vol. 10, no. 5, p. 1824, 2020.

[15] F. D'Agostino, F. Silvestro, K. P. Schneider, C.-C. Liu, Y. Xu, and D. T. Ton, "Reliability assessment of distribution systems incorporating feeder restoration actions," in *2016 Power Systems Computation Conference (PSCC)*, pp. 1–7, 2016.

[16] M. Mukherjee, S. Poudel, A. Dubey, and A. Bose, "A framework to quantify the value of operational resilience for electric power distribution systems," in *2020 IEEE/PES Transmission and Distribution Conference and Exposition (T&D)*, pp. 1–5, 2020.

[17] "IEEE Guide for Electric Power Distribution Reliability Indices," 2012.

[18] H.-G. Yeh, D. F. Gayme, and S. H. Low, "Adaptive var control for distribution circuits with photovoltaic generators," *IEEE Transactions on Power Systems*, vol. 27, no. 3, pp. 1656–1663, 2012.

[19] Gurobi Optimization, LLC, "Gurobi Optimizer Manual," 2024.

[20] P. H. Larsen, K. Carney, J. H. Eto, G. Jiang, D. Joshi, *et al.*, "ICE Calculator 2.0: Final Report for Phase 1 of the National Initiative to Update the Interruption Cost Estimate (ICE) Calculator," 2025.

979-8-3315-8138-1